Molecular Biology of the Cell
Vol. 18, 3119–3130, August 2007

Multiple Receptor Interactions Trigger Release of Membrane and Intracellular Calcium Stores Critical for Herpes Simplex Virus Entry

Natalia Cheshenko,* Wen Liu,* Lisa M. Satlin,* and Betsy C. Herold*†

Departments of *Pediatrics and †Microbiology, Mount Sinai School of Medicine, New York, NY 10029

Submitted January 26, 2007; Revised May 1, 2007; Accepted May 29, 2007
Monitoring Editor: Adam Linstedt

Herpes simplex viruses (HSV) harness cellular calcium signaling pathways to facilitate viral entry. Confocal microscopy and small interfering RNA (siRNA) were used to identify the source of the calcium and to dissect the requisite viral–cell interactions. Binding of HSV to human epithelial cells induced no calcium response, but shifting the cells to temperatures permissive for penetration triggered increases in plasma membrane calcium followed by a global release of intracellular calcium. Transfection with siRNA targeting the proteoglycan syndecan-2 blocked viral binding and abrogated any calcium response. Transfection with siRNA targeting nectin-1, a glycoprotein D receptor, also prevented both membrane and intracellular calcium responses. In contrast, the membrane response was preserved after transfection with siRNA targeting integrinαv, a novel glycoprotein H receptor. The membrane response, however, was not sufficient for viral entry, which required interactions with integrinαv and release of inositol-triphosphate receptor-dependent intracellular calcium stores. Thus, calcium plays a critical, complex role in HSV entry.

INTRODUCTION

Herpes simplex viruses (HSV) are a global health problem and the leading cause of genital ulcers, neonatal encephalitis, and a major cofactor for human immunodeficiency virus infection. Development of novel strategies to prevent infection requires elucidation of the molecular and cellular events critical for entry. Previous work demonstrates that viral entry is a complex process that requires multiple interactions at the cell surface involving four envelope glycoproteins, gD, gB, and heterodimers of gH–gL. The number of glycoproteins required illustrates the complexity of HSV entry compared with that observed with most other viruses, which typically require one or at most two glycoproteins. The cascade is initiated by binding of HSV to heparan sulfate proteoglycans at the cell surface; glycoprotein C plays the major role in mediating binding for HSV-1, whereas gB plays the dominant role in mediating binding for HSV-2 (Herold *et al*., 1991; Cheshenko and Herold, 2002). After engagement of this attachment receptor, gD interacts with one of several coreceptors, of which nectin-1 may play the predominant role on human epithelial cells (Linehan *et al*., 2004). Independently of its role in attachment, gB is also required for fusion as are heterodimers of gH–gL (Spear, 2004). Accumulating evidence points to gH as the executor of fusion, in part, because it exhibits structural–functional features typical of fusion proteins, including a fusion peptide and heptad repeat segments able to form coiled coils (Gianni *et al*., 2005, 2006). However, no receptor for gH has been definitively identified. Precisely how these interactions trigger viral entry is not clear. The concentration of intracellular free Ca^{2+} ($[Ca^{2+}]_i$) regulates a variety of cellular processes, including sperm–egg fusion, contraction, secretion, cell growth, and apoptosis (Berridge, 2005). The specificity of Ca^{2+} responses is characterized by the frequency, amplitude, duration, and spatial restriction of the Ca^{2+} signaling (Berridge, 2005). Intracellular Ca^{2+} signals may be localized to domains at or just below the plasma membrane (referred to as membrane Ca^{2+}), or they may be associated with release from the endoplasmic reticulum (ER) and mitochondria. We previously reported that HSV-1 and HSV-2 trigger the release of Ca^{2+} and that Ca^{2+} signaling plays a critical role in viral entry (Cheshenko *et al*., 2003). Pharmacological inhibition of the inositol-triphosphate receptor (IP_3R) or chelation of intracellular Ca^{2+} abrogated the Ca^{2+} response measured by fluorometry, and it prevented viral infection (Cheshenko *et al*., 2003). Additionally, activation of Ca^{2+} signaling was associated with phosphorylation of focal adhesion kinase (FAK), which facilitated transport of viral capsids to the nuclear pore (Cheshenko *et al*., 2005). These findings suggest that HSV may hijack Ca^{2+} signaling pathways to trigger entry. Building from this framework, the current studies used confocal microscopy and small interfering RNA (siRNA) to define the Ca^{2+} response to HSV-1 and HSV-2, the viral–cell interactions required, and their role in triggering Ca^{2+} signaling and viral entry. Results indicate that binding to syndecan-2, a major heparan sulfate proteoglycan, and nectin-1 are sufficient to trigger increases in membrane Ca^{2+}, but engagement of integrinαv and release of IP_3R-dependent intracellular Ca^{2+}stores are required to complete the entry process.

This article was published online ahead of print in *MBC in Press* (http://www.molbiolcell.org/cgi/doi/10.1091/mbc.E07–01–0062) on June 6, 2007.

Address correspondence to: Betsy C. Herold (betsy.herold@mssm.edu).

Abbreviations used: $[Ca^{2+}]_i$, intracellular calcium ion concentration; HSV, herpes simplex virus(es); IP_3R, inositol triphosphate receptor; pi, postinfection; pfu, plaque-forming unit; siRNA, small interfering RNA.

MATERIALS AND METHODS

Cells and Viruses

CaSki (human cervical) and Chinese hamster ovary (CHO)K1 cells were passaged in DMEM supplemented with 10% fetal bovine serum. ECC1 (human uterine epithelial) cells (Schaefer *et al*., 2004) were passaged in DMEM/F-12 media (Invitrogen, Carlsbad, CA). For polarization, the ECC1 cells were plated on 0.4-μm pore size, 12-mm-diameter collagen-coated inserts (Corning Life Sciences, Acton, MA) (Galen *et al*., 2006). HSV-2(G), HSV-1(KOS), and HSV-1(K26GFP), which contains a green fluorescent protein (GFP)–VP26 fusion protein (Desai and Person, 1998), were grown on Vero cells. Stocks of HSV-1(KOS)gH$^-$, in which the *Escherichia coli* galactosidase gene replaces part of the gH open reading frame (Novotny and Spear, unpublished data), were propagated on complementing F6 cells (Forrester *et al*., 1992). Stocks of HSV-1(KOS)gD6, a gD-negative virus (Warner *et al*., 1998) were propagated on the complementing VD60 cells (Ligas and Johnson, 1988) and stocks of HSV-2(G)gB2$^-$, a gB-2 deletion virus, were propagated on VgB2 cells (Cheshenko and Herold, 2002). One passage of each of the deletion viruses through Vero cells yields glycoprotein-negative virions.

Viral Labeling and Purification

Purified DiD-labeled virus was prepared by infecting Vero cells with each of the viral variants at a multiplicity of infection (moi) of 0.001 plaque-forming units (pfu)/cell for replication-competent viruses and 1 pfu/cell based on the viral titer on complementing cells for the deletion viruses. Cells were harvested 48 h postinfection (pi) for replication-competent and 16 h pi for deletion viruses, and then they were incubated with lipophilic tracer DiD (Invitrogen) at 1 μM for 10 min at room temperature before purification on sucrose gradients (Tuyama *et al*., 2006). Viral titers were determined by plaque assays and relative viral particle numbers by preparing Western blots of purified viral preparations and probing for expression of viral gD and/or gB (Cheshenko and Herold, 2002). For studies with deletion viruses, cells were infected with ~100–500 particles/cell, which is equivalent to an moi of 10 pfu/cell for the parental strains HSV-2(G) and HSV-1(KOS), respectively.

siRNA Transfections

Cells were transfected with 100 pmol/well (12-well plates) of the indicated siRNA by using the Effectene transfection reagent (QIAGEN, Valencia, CA) as described previously (Cheshenko *et al*., 2005). The siRNAs used were syndecan-2 (12528, 12618, 12433), IP_3R type I (106735), IP_3R type II (111123), IP_3R type III (111127), integrinαv, ITGAV (111118, 106732, 106731) HVEM (111369, 13868, 214894), or nonspecific siRNA (Silencer Negative control #1), all from Ambion (Austin, TX). The nectin siRNA was prepared by Dharmacon RNA Technologies (Lafayette, CO) (Galen *et al*., 2006). Cells were analyzed for protein expression 48 h after transfection by preparing Western blots and by immunohistochemistry and confocal microscopy. Cells were infected with HSV 48 h after transfection, and infection was monitored by plaque assays.

Antibodies

Antibodies and dilutions were as follows: rabbit anti-IP_3R type I and anti-IP_3R type II diluted 1:200 (PA1-901 and PA1-904, respectively; Affinity Bioreagents, Golden, CO); anti-nectin murine monoclonal antibodies (mAbs) CK41 and CK6, diluted 1:500 (gift from R. Eisenberg and G. Cohen, University of Pennsylvania) (Galen *et al*., 2006, see reference 27); anti-integrinαv mAb diluted 1:500 (407288; Calbiochem, San Diego, CA); anti-syndecan-2 mAb diluted 1:200 (34164 B-A38; Abcam, Cambridge, MA); anti-syndecan-1 goat polyclonal antibody (Ab) diluted 1:200 (BAF2780; R&D Systems, Minneapolis, MN); anti-VP16 diluted 1:500 (sc7545; Santa Cruz Biotechnology, Santa Cruz, CA); anti-VP5 mAb diluted 1:200 (sc13525; Santa Cruz Biotechnology); anti-β-actin diluted 1:1000 (A-5441; Sigma-Aldrich, St. Louis, MO); anti-histone H1 diluted 1:10000 (sc-8030; Santa Cruz Biotechnology); and anti-golgin97 diluted 1:500 (A-21270; Invitrogen). The secondary Ab for Western blots was horseradish peroxidase-conjugated goat anti-mouse diluted 1:500 (Calbiochem), and for confocal microscopy, it was Alexa Fluor 488-conjugated anti-mouse secondary Ab diluted 1:1000 (Invitrogen).

Synchronized Infection, Binding, and VP16 Assays

Cells were precooled and exposed to virus at 4°C for 4 h to allow binding. Unbound virus was removed by washing, and the cells were transferred to 37°C to allow viral penetration for 15 min. Bound virus that had not penetrated was inactivated by washing the cells with a low pH citrate buffer (50 mM Na-citrate and 4 mM KCl, adjusted to pH 3.0) for 2 min and then washing three times with phosphate-buffered saline (PBS). The cells were then overlaid with fresh medium. For binding studies, cells were exposed to purified virus for 5 h at 4°C. Unbound virus was removed by washing, and the cell-bound virus analyzed by preparing Western blots of cell lysates and probing with anti-gD mAb 1103 (Virusys, Sykesville, MD) (Cheshenko and Herold, 2002). To examine transport of VP16 to the nucleus, nuclear extracts were prepared 1 h after infection and analyzed by preparing Western blots as described previously (Cheshenko *et al*., 2003).

Confocal Microscopy

Cells were grown on glass coverslips in 12-well plates, transfected with siRNA as described above, and, if indicated, infected 48 h after transfection with HSV at the noted moi in a synchronized infection assay. To label plasma membranes, the cells were stained for 30 min with EZ-Link sulfosuccinimidobiotin (EZ-Link SuLfo-NHS-Biotin) reagent (0.1 mM; Pierce Chemical, Rockford, IL), which reacts with primary amines on cell-surface proteins before infection, fixed with 4% paraformaldehyde solution (Electron Microscopy, Hatfield, PA) at indicated times pi, and the biotinylated cells were reacted with Alexa Fluor 546- or 350-conjugated streptavidin antibody (1:1000 dilution; S11225, S11249; Invitrogen). Nuclei were detected by staining with 4,6-diamidino-2-phenylindole (DAPI) nucleic acid stain (Invitrogen). To visualize syndecan, nectin, integrins, IP_3Rs, or VP5, cells were permeabilized with 1% Triton X after fixation, incubated with the appropriate primary Abs and subsequently with an Alexa Fluor 488-conjugated anti-mouse secondary Ab. To visualize Ca^{2+}, the cells were loaded with 10 μM Calcium Green TM-1 AM (C 301I; Invitrogen) for 30 min at 37°C, extracellular Ca^{2+} was removed by washing three times with Ca^{2+}-free PBS. Images were examined using a Zeiss LSM 510 Meta confocal microscope (Carl Zeiss, Thornwood, NY) fitted with Plan-Apochromat 100×/1.4 oil immersion objective. Images were captured in an optical slice of ~1 μm with appropriate filters. Alexa FlourR 488, Calcium Green, and GFP were excited using the 488-nm line of a kypton/argon laser and viewed with a 505- to 530-nm band pass filter; AlexaFluor 547R and Vybrant DiI were excited using the 543-nm line of helium/neon laser and collected with a 560- to 615-nm long-pass filter; Alexa Fluor 647 DiD 633 were excited with the 633-nm line red helium/neon laser and collected with long-pass 650 filter; AlexaFluor 360 were excited with 405-nm diode laser and collected with a 420- to 480-nm filter. All images were captured using the multitrack mode of microscope to decrease cross talk of fluorescent signals. Z-sections were captured in an optical slice of 0.23 μm. Image analysis and subcellular localization were evaluated using the LSM confocal software package (Carl Zeiss). Quantification of cell-associated GFP, Calcium Green, or DiD was performed with NIH Image densitometric software (100 cells analyzed and counted; National Institutes of Health, Bethesda, MD). Images of polarized cells were captured in series of optical slices 0.5 and 1.5 μm starting from the apical membrane. Three-dimensional (3-D) images were generated using the Volocity 4 confocal software (Improvision, Lexington, MA). For live image microscopy, cells were grown in Delta T dishes 0.17 mm (product no. 1207107; Fisher Scientific, Pittsburgh, PA) and labeled with VYBRANT-DiI (V22889; Invitrogen). Then, they were loaded with Calcium Green for 4 h at 4°C, and infected with virus for 4 h at 4°C. Finally, extracellular Ca^{2+} and unbound virus were removed by washing three times with PBS, overlaid with 25 mM HEPES buffer, and cells were placed into a temperature-regulated Delta T chamber in a Zeiss LSM 510 Meta confocal microscope fitted with a 100×/1.4 oil objective. Images were obtained when the temperature in the chamber reached 37°C; 20 consecutive images of the same field were obtained at the indicated times. Channel 1 for DiD (emission 633) was converted to blue color for presentation of images.

Measurement of $[Ca^{2+}]_i$ by Fluorometry

Transfected cells were loaded with 10–20 μM fura-2 acetoxymethyl ester prepared in perfusate buffer for 30–60 min. Then, cells were rinsed with fresh buffer for 30 min at 37°C and exposed sequentially to PBS or HSV at the specified moi. Using a Nikon Eclipse TE300 inverted epifluorescence microscope (Nikon, Tokyo, Japan) linked to a cooled Pentamax charge-coupled device camera (Princeton Scientific Instruments, Monmouth Junction, NJ) interfaced with a digital imaging system (MetaFluor, Molecular Devices, Downingtown, PA), $[Ca^{2+}]_i$ was measured in 8–15 individually identified cells as previously described (Cheshenko *et al*., 2003). Images were acquired every 2–10s for 5–10 min before and then 10 min after the addition of PBS or virus. Eight to 15 cells were monitored for each experiment.

RESULTS

HSV Triggers Both Membrane and Intracellular Global Ca^{2+} Stores

We exploited confocal microscopy to monitor HSV entry. CaSki or CHOK1 cells were mock infected or infected with purified KVP26GFP, an HSV-1 variant expressing a VP26–GFP fusion capsid protein, in which the viral envelope was also labeled with a fluorescent long-chain carbocyanine dye DiD (Lakadamyali *et al*., 2003; Le Blanc *et al*., 2005). This enabled discrimination between viral envelopes and capsids. The cells were fixed following binding (4°C for 4 h), entry (15 min after temperature shift to 37°C), or 1 h after entry (1 h after inactivating bound virus that had not penetrated with a low pH buffer). Bound viral envelopes (red) were readily detected on both CaSki and CHOK1 cells at 4°C

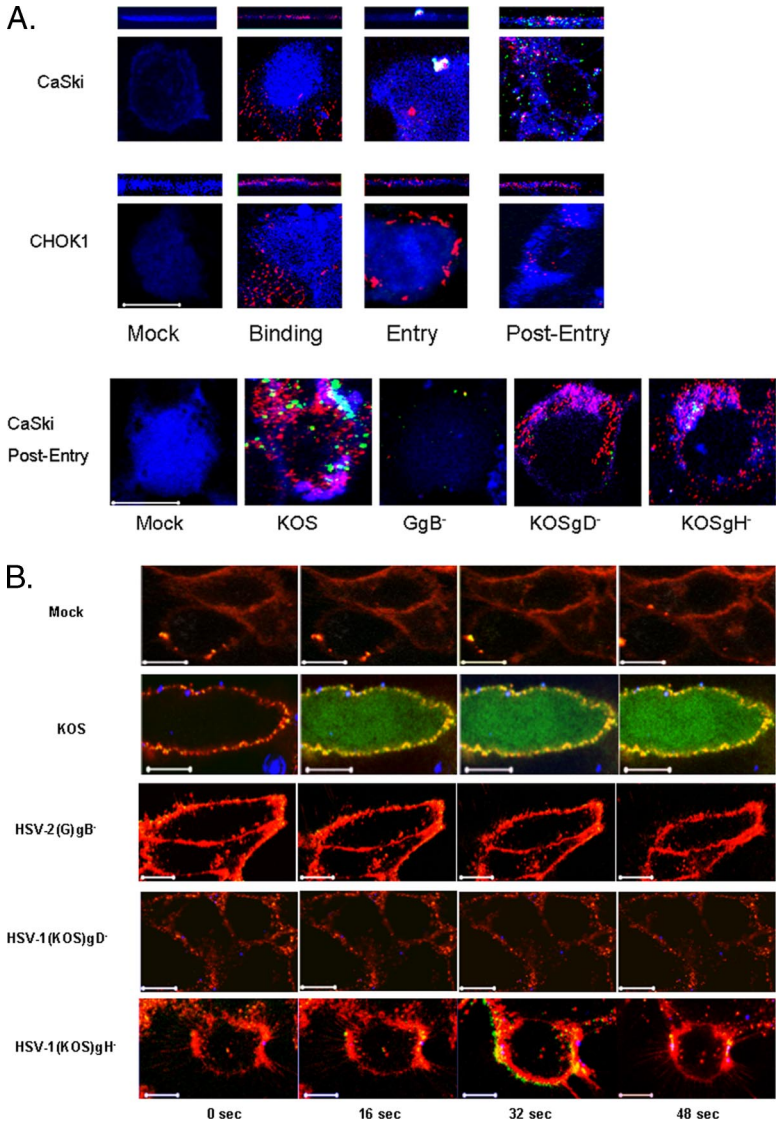

Figure 1. HSV enters CaSki, but not CHO-K1, cells, and it elicits an increase in both membrane and global intracellular Ca^{2+}. (A) CaSki or CHO-K1 cells were exposed to DiD-envelope–labeled HSV-1(KV26GFP) virus (moi = 10 pfu/cell) in a synchronized assay, and then they were examined by confocal microscopy. Plasma membranes stained with EZ-Link are blue, DiD-stained viral envelopes are red, and GFP-tagged viral capsid proteins are green. Bottom, CaSki cells were mock infected or exposed to DiD-labeled wild-type or deletion viruses (moi = 10 pfu/cell for wild-type and an equivalent number of viral particles for the deletion viruses) in a synchronized assay, fixed, permeabilized, and stained for the viral capsid protein VP5 (green) 1 h after entry. Areas of colocalization between cell membrane and envelope look turquoise. Images are representative of 100 cells. Bar, 10 μm. (B) CaSki cells were loaded with Calcium Green and mock infected or infected with each of the DiD-labeled viruses. Live images acquired every 2 s beginning immediately after the temperature reached 37°C. For these images, the plasma membrane is red, viral envelopes are blue, and Ca^{2+} is green; colocalization of Ca^{2+} and plasma membrane is yellow.

(Figure 1A). After a shift to 37°C, a temperature permissive for penetration, fusion of the viral envelope with cell membrane was observed and by 1 h after entry, viral capsids (green) were readily detected intracellularly in CaSki cells. In contrast, no fusion or intracellular delivery of viral capsids was observed in CHOK1 cells, which are permissive for HSV binding only because the cells lack gD coreceptors (Montgomery *et al*., 1996). To further validate the confocal model, studies were conducted with viral variants deleted in specific envelope glycoproteins. CaSki cells were infected with DiD-labeled purified parental virus [HSV-1(KOS) or HSV-2(G)] or viruses deleted in HSV-2 gB (GgB^-), HSV-1 gD (KOSgD-1^-), or HSV-1 gH (KOSgH-1^-) in a synchronized infection assay. Cells were fixed, permeabilized, and stained with a mAb to the viral capsid protein VP5 either immediately after binding or 1 h posttemperature shift. Representative images obtained 1 h after entry are shown in Figure 1A, bottom. Consistent with the results obtained with the dually labeled KVP26GFP virus, fusion of the envelope (red) with the membrane (blue) and intracellular delivery of VP5 (green) was readily detected after infection of CaSki cells with KOS. Similar results were observed with HSV-2(G) (data not shown). In contrast, no cell-associated virus was detected after exposure to HSV-2(G)gB^- virus, consistent with previous studies demonstrating that gB plays a critical role in HSV-2 binding (Cheshenko and Herold, 2002). Cell-bound virus was detected after infection with HSV-1 variants deleted in either gD-1 or gH-1, but no delivery of VP5 was observed. These findings are consistent with the essential roles played by gD and gH in mediating entry for both serotypes after binding. To examine the Ca^{2+} response during the entry process, CaSki cells were loaded with Calcium Green and mock infected or infected with an equivalent number of viral particles each of the purified DiD-labeled viruses in a synchronized assay. For presentation of these images, the plasma membranes are red and viral envelopes are blue (Figure 1B). Live confocal images were acquired every 2 s immediately after the temperature reached 37°C. Temperature–kinetic studies demonstrated that viral entry occurs before the temperature reaches 37°C. Cells were exposed to virus at 4°C, washed, and then shifted to different temperatures. At various times posttemperature shift, nonpenetrated virus was inactivated with a low pH buffer (or pH 7.4 buffer as a control), and infection was monitored by counting plaques 48 h pi (Gerber *et al*., 1995). Entry is most efficient at 37°C, with 50% of HSV-2(G) enter-

ing within 7 min. At room temperature, 50% of virus is internalized in 20 min and at 18°C, 25% of virus enters cells within 40 min (data not shown). These findings are consistent with the confocal images (Figure 1B). Images acquired immediately after HSV-1(KOS)–infected cells reached 37°C already demonstrated an increase in membrane Ca^{2+}. The microscopic techniques used in this study do not allow the definitive localization of the membrane Ca^{2+} signal. Within 16 s after reaching 37°C, an increase in global intracellular Ca^{2+} was also observed, which persisted for 5–10 min. In contrast, no change in membrane or global Ca^{2+} was observed at any time after exposure to the HSV-2(G)gB^- virus, which is impaired in binding and entry. Bound virus was detected following exposure to gD^- virus, but the virus failed to elicit any Ca^{2+} response. In contrast, some increase in membrane Ca^{2+} was observed after exposure to the gH^- virus, but no global intracellular Ca^{2+} response was detected. Together, these findings indicate that there are two distinct Ca^{2+} stores activated in response to HSV. Increases in Ca^{2+} at the membrane require viral binding (gB) and engagement of coreceptors (gD), whereas release of global intracellular stores also requires gH–gL.

Identification of Cellular Components Required for Viral Entry

Building from these observations, we next focused on the cellular components that contribute to the signaling response. The initial contact of HSV with epithelial cells is binding to heparan sulfate chains of cell surface proteoglycans, but the core proteins involved have not been identified. Transmembrane heparan sulfate proteoglycans include glypican, cerebroglycan, betaglycan, CD44, and members of

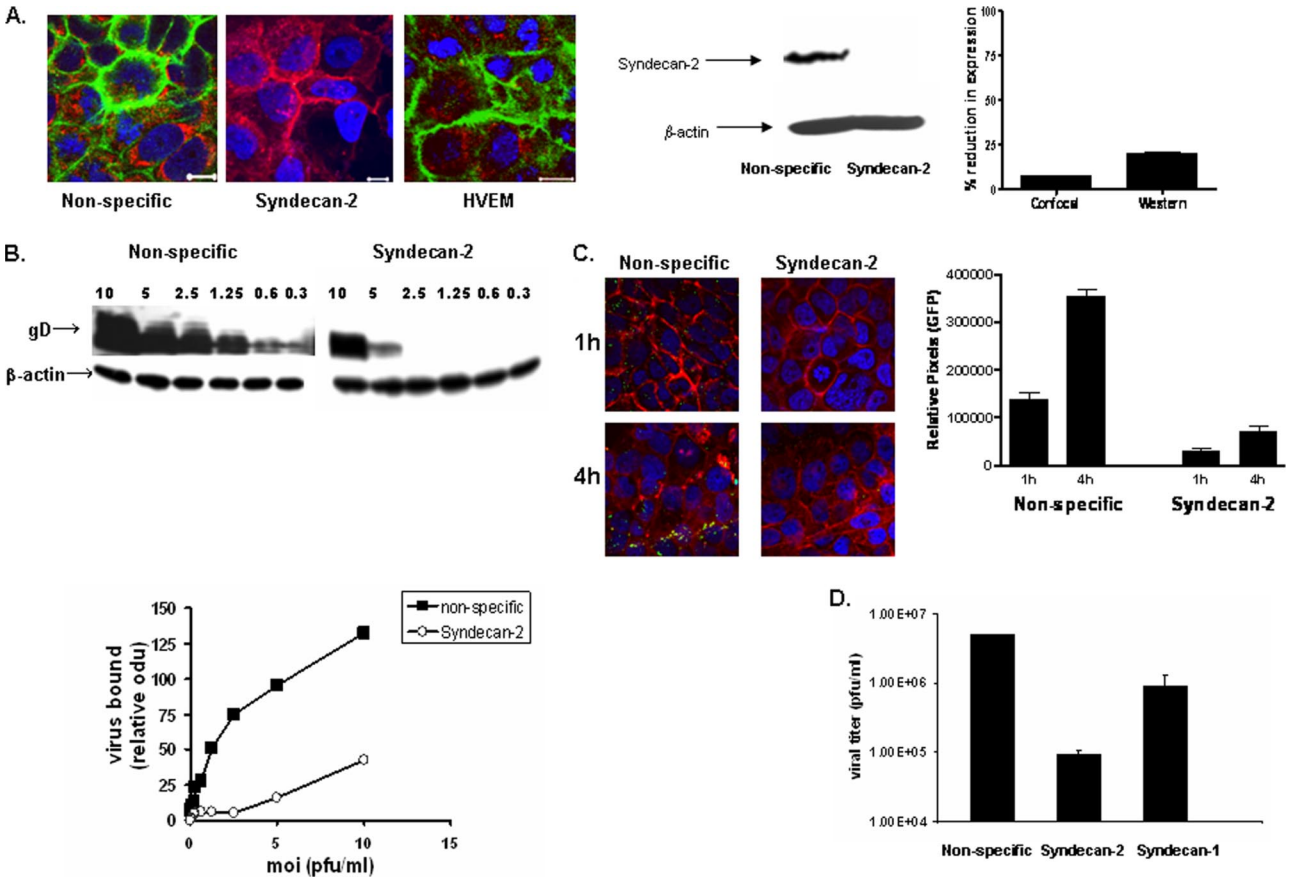

Figure 2. Knockdown of syndecan-2 expression with siRNA inhibits viral binding and infection. (A) Cells were transfected with nonspecific, HVEM-specific, or syndecan-2–specific siRNA. Forty-eight hours after transfection, they were stained with anti-syndecan Abs (green), and then they were examined by confocal microscopy; plasma membranes were stained with EZ-Link (red) and nucleic acids were stained with DAPI (blue) (left). Alternatively, cell lysates were prepared 48 h after transfection, and then proteins were separated, transferred by Western blotting, and incubated with anti-syndecan mAb. Blots were then stripped and reprobed with mAb to β-actin. Representative blots from three independent experiments are shown (middle). Blots were scanned and relative amounts of syndecan-2 compared by optical densitometry (right). For each confocal experiment, 100 cells were counted, and the percentage of cells expressing syndecan in siRNA-transfected cells relative to expression in cells transfected with nonspecific siRNA was compared (right). (B) Transfected CaSki cells were exposed to serial dilutions of HSV-2(G) at the moi indicated for 5 h at 4°C. The cell-bound viral particles were detected by analyzing Western blots of cell lysates for gD; blots were also probed with a mAb to β-actin to control for cell loading. The graph shows relative viral particles bound at each moi, and it is representative of results obtained in three independent experiments conducted in duplicate. (C) Transfected CaSki cells were infected with K26GFP virus (moi = 5) and 1- and 4 h pi, the cells were fixed, stained, and viewed by confocal microscopy (red; plasma membrane, blue, nuclei; green, viral VP26). Results are representative of three independent experiments. The relative amount of intracellular GFP was compared by collecting data from ~100 cells from different fields using NIH Image software. Results are expressed as the pixel intensity per cell in relative units. (D) Cells transfected with nonspecific, syndecan-2 or syndecan-1 specific siRNA were exposed to serial dilutions of HSV-2(G). Plaques were counted 48 h pi and viral titer (pfu/ml) determined. Results are means ± SD of three independent experiments conducted in duplicate.

the syndecan family. Recent studies indicate that the predominant proteoglycans on human genital epithelial cell surfaces are syndecan-1 and syndecan-2 (Bobardt *et al.*, 2007). We confirmed these findings by examining CaSki cells for the expression of syndecan-1, syndecan-2, and glypican by Western blotting and confocal microscopy. Syndecan-2 predominated with no glypican detected (data not shown). Transfection of CaSki cells with syndecan-2 sequence-specific siRNA markedly reduced syndecan-2 expression 48 h after transfection as illustrated by scanning of confocal microscopy images or Western blots, whereas transfection with the unrelated HVEM sequence-specific siRNA had no effect on syndecan-2 expression (Figure 2A). The effect of syndecan gene silencing on infection was monitored by microscopy using K26GFP or plaque assays. CaSki cells were transfected with nonspecific or syndecan-2 siRNA, and then 48 h later, they were infected with K26GFP (5 pfu/cell). One and 4 h pi, the cells stained with EZ-Link SuLfo-NHS-Biotin to detect plasma membranes, and then the cells were fixed and stained with DAPI to detect nuclei and viewed by confocal microscopy. Viral GFP is detected in the cytoplasm of CaSki cells as early as 1 h pi, and it increases in intensity by 4 h, consistent with a productive infection (Figure 2B). In contrast, no intracellular GFP is detected in cells transfected with syndecan-2–specific siRNA. Parallel studies demonstrate that transfection with syndecan-specific siRNA reduced viral binding by >90% (Figure 2C) and inhibited viral plaque formation by 98% (Figure 2D). Transfection with syndecan-1–specific siRNA had more modest effects and reduced infection by 82%, suggesting that syndecan-1 also plays a role as a core proteolycan for viral binding (Figure 2D). Together, these findings demonstrate for the first time a role for syndecans as core proteoglycan proteins important for HSV infection of human cervical epithelial cells. The next

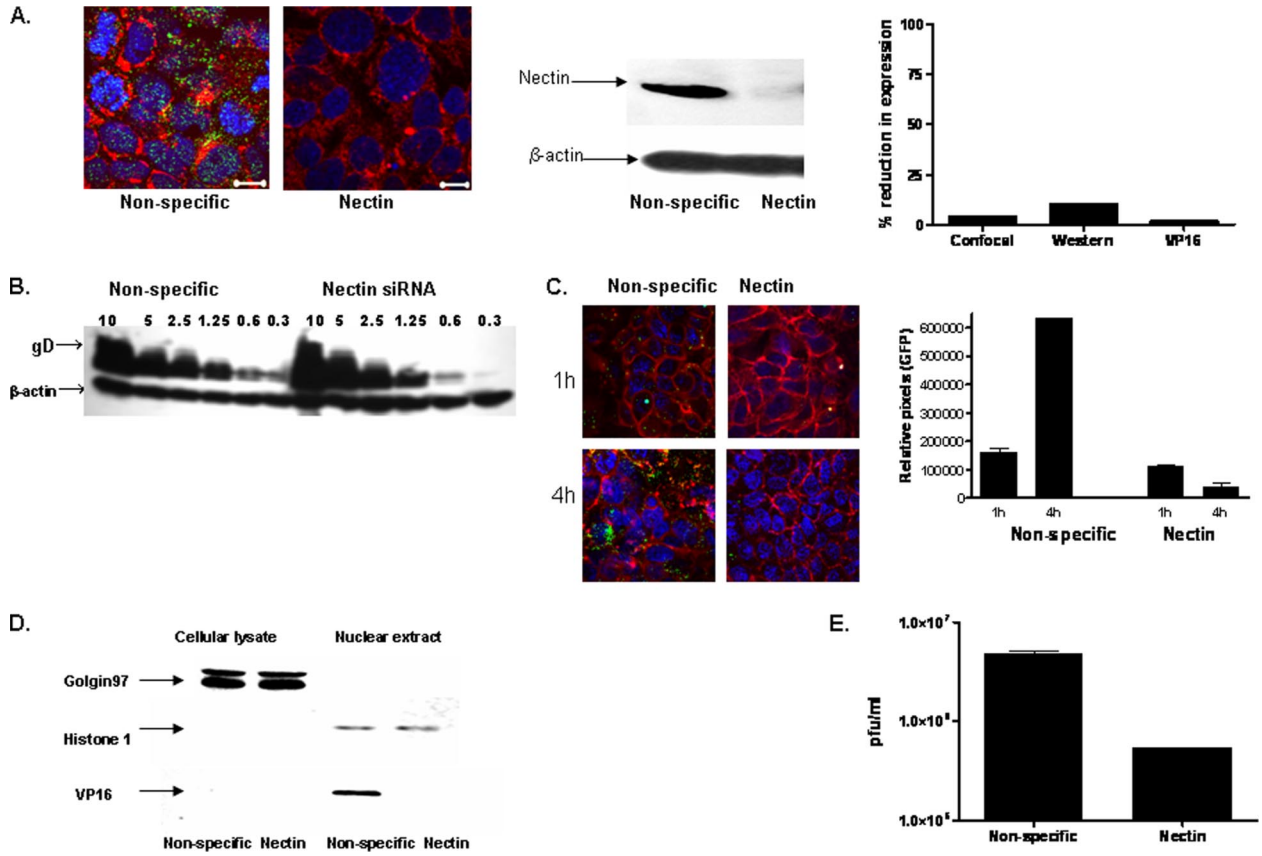

Figure 3. Blockade of nectin-1 by siRNA prevents viral entry after binding. (A) Cells were transfected with nonspecific or nectin-1–specific siRNA and 48 h after transfection, they were stained with a cocktail of anti-nectin-1 Abs (green) and examined by confocal microscopy (plasma membranes, red; nucleus, blue) (left). Alternatively, cell lysates for Western blotting were prepared 48 h after transfection, and then they were incubated with anti-nectin mAbs, stripped, and reprobed with mAb to β-actin. Representative blots from three independent experiments are shown (middle). Blots and confocal images were quantified as described for Figure 2. (B) Transfected CaSki cells were exposed to serial dilutions of HSV-2(G) at the moi indicated for 5 h at 4°C. The cell-bound viral particles were detected by analyzing Western blots of cell lysates for gD; blots were also probed with a mAb to β-actin to control for cell loading. The blot is representative of three independent experiments. (C) Transfected cells were infected with K26GFP virus (moi = 5) and 1 and 4 h after infection, the cells were fixed, stained, and viewed by confocal microscopy (red; plasma membrane, blue, nuclei; green, viral capsids). Results are representative of three independent experiments. The relative amount of intracellular GFP was compared by collecting data from ~100 cells from different fields using NIH Image J software. Results are expressed as the pixel intensity per cell in relative units. (D) Transfected CaSki cells were exposed to HSV-2(G) (moi = 1) in a synchronized infection assay, and cell lysates and nuclear extracts were prepared 1 h after infection and analyzed for presence of viral tegument protein VP16 by Western blotting. Blots were also probed for the cytosolic protein, golgin 97, and the nuclear protein, histone H1 Results shown are representative of three independent experiments. Blots were scanned, and nuclear VP16 detected in nectin-siRNA–transfected cells as a percentage of VP16 detected in nonspecific siRNA-transfected cells was compared (A, right). (E) The transfected cells were exposed to serial dilutions of HSV-2(G). Plaques were counted 48 h pi, and viral titer was determined. Results are means ± SD of three independent experiments conducted in duplicate.

step in viral entry is binding of gD to a coreceptor. Several studies suggest that nectin-1 is the major coreceptor on human epithelial cells (Linehan *et al.*, 2004; Galen *et al.*, 2006). Transfection of cells with nectin-1 sequence-specific, but not HVEM-specific, siRNA reduced its expression by at least 90% (based on scanning of confocal microscopy images and Western blots) (Figure 3A). Binding of virus was not impaired (Figure 3B), but no viral entry was detected in cells transfected with nectin siRNA by confocal microscopy using K26GFP virus (Figure 3C). Moreover, nuclear transport of VP 16, a viral tegument protein, was also reduced by 98% (Figure 3D), and viral plaque formation was reduced by 90% (Figure 3E). These findings confirm an important role for nectin-1 in facilitating HSV infection of human epithelial cells. The heterodimeric complex of gH–gL is also required for viral entry. Although no gH–gL receptor has been definitively identified, several studies suggest a possible role for integrins. For example, a soluble form of HSV-1 gH–gL bound to Vero cells and mutation of a potential integrin-binding motif, Arg-Gly-Asp (RGD), in gH abolished the binding (Parry *et al.*, 2005). Consistent with the possible role of integrins in HSV entry is the observation that binding of many ligands to integrins triggers Ca^{2+} signaling pathways (Giancotti and Ruoslahti, 1999). To explore the possible role of αv integrins in HSV entry, CaSki cells were transfected with integrinαv siRNA, which reduced integrin expression by 63–83% (Figure 4A). Controls included cells transfected with HVEM siRNA, which had no impact on integrinαv expression (data not shown). Confocal microscopy studies with purified dually labeled K26GFP virus demonstrated that the viral envelope (blue) merged with the cell membrane (red), but the virus was retained within the membrane and failed to release viral capsids (green); in contrast, release of capsids was readily detected in cells transfected with nonspecific siRNA, and by 4 h pi, intracellular GFP was readily detected (Figure 4B). Consistent with the block in infection observed by microscopy in Figure 4B, nuclear transport of VP 16 was also reduced by 74% (Figure 4A, left) and viral yields were reduced by 94% in a plaque assay (Figure 4C). Together, these findings demonstrate that integrinαv plays a role in viral entry, possibly through engagement of gH. To address whether gH might be mediating the binding to integrinαv, cells were mock infected or infected with ~100 particles/cell of purified labeled gD^- or

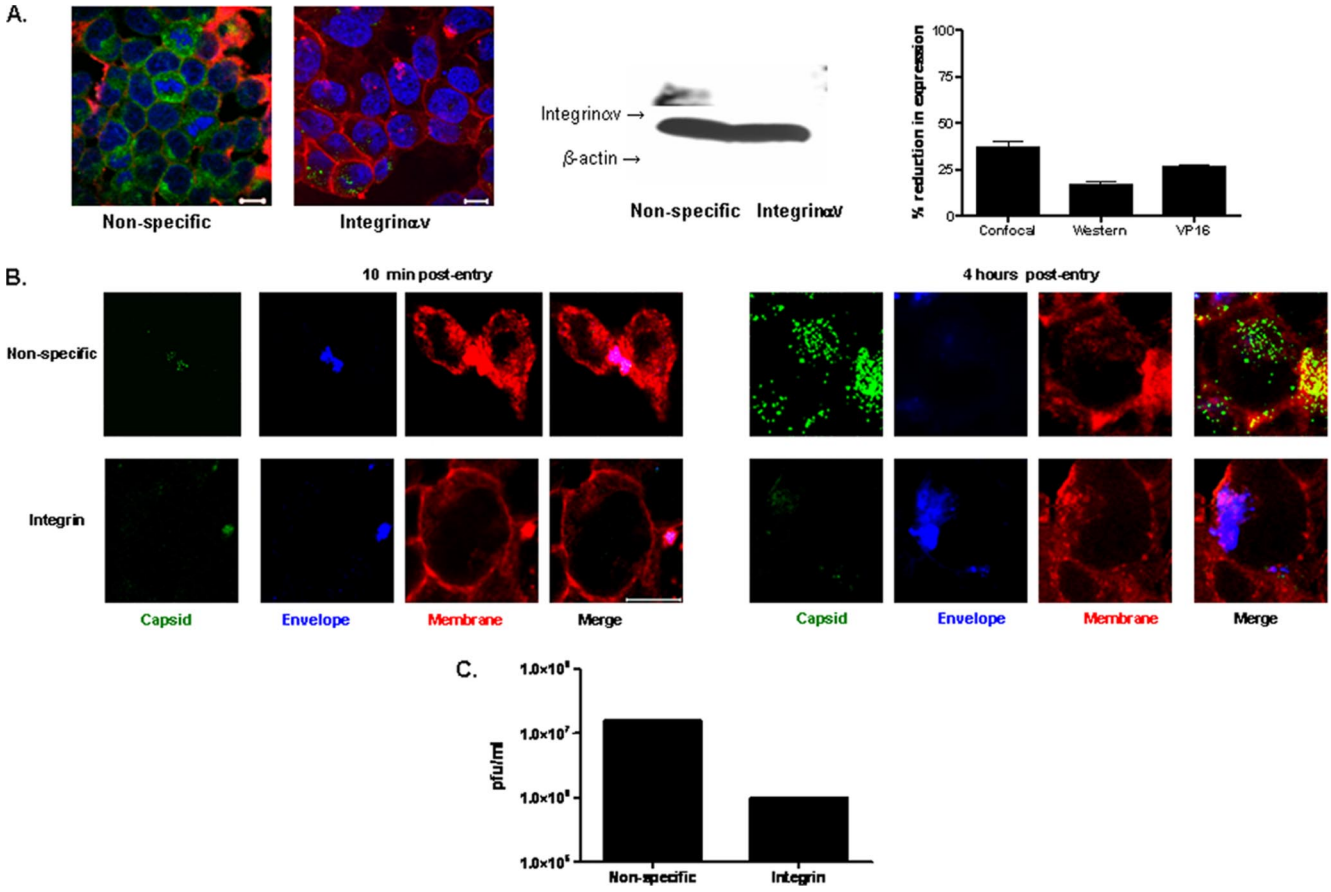

Figure 4. Integrinαv interacts with virus to facilitate viral entry and infection. (A) Cells were transfected with nonspecific or integrinαv-specific siRNA, and 48 h after transfection, cells were stained with a mAb specific for integrinαv subunits (integrin, green; plasma membrane, red; and nuclei, blue). Alternatively, Western blots of cell lysates were prepared 48 h after transfection. Representative blots from three independent experiments are shown (middle). Blots and confocal images were quantified as described for Figure 2 (right). The graph also shows nuclear VP16 detected in nectin-siRNA–transfected cells as a percentage of VP16 detected in nonspecific siRNA-transfected cells as described in Figure 3. (B) Transfected CaSki cells were infected with DiD-envelope labeled K26GFP virus (moi = 5 pfu/cell), and 10 min and 4 h after infection, the cells were fixed, stained, and viewed by confocal microscopy (viral capsid, green; plasma membrane, red; and viral envelopes, blue). Areas of colocalization of plasma membrane and viral envelope are purple. Results are representative of three independent experiments. (C) The transfected cells were exposed to serial dilutions of HSV-2(G). Plaques were counted 48 h pi, and viral titer was determined. Results are means ± SD of three independent experiments conducted in duplicate.

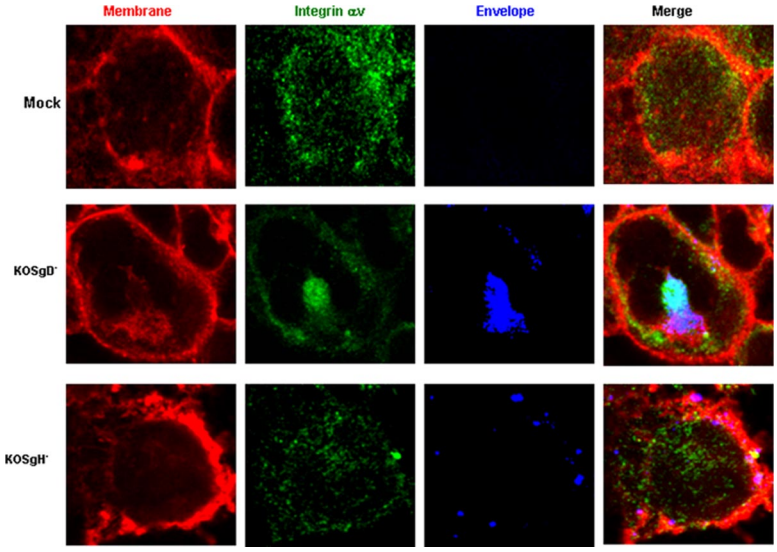

Figure 5. Interactions with integrinαv requires viral gH. Transfected CaSki cells were mock infected or infected with purified DiD-envelope labeled gD^- or gH^- virus (viral particle numbers equivalent to moi = 10 pfu/cell) in a synchronized assay and fixed and stained for integrinαv 15 min after the temperature reached 37°C. Areas of colocalization between integrinαv (green) and viral envelopes (blue) are turquoise, and areas of colocalization between the plasma membrane (red) and viral envelope (blue) are purple. Results are representative of those obtained with ~100 cells in five independent experiments.

gH^- virus. The cells were fixed 15 min posttemperature shift, and then they were stained with a mAb to integrinαv (Figure 5). In the mock-infected cells, integrinαv is diffusely distributed near the plasma membrane. After exposure to

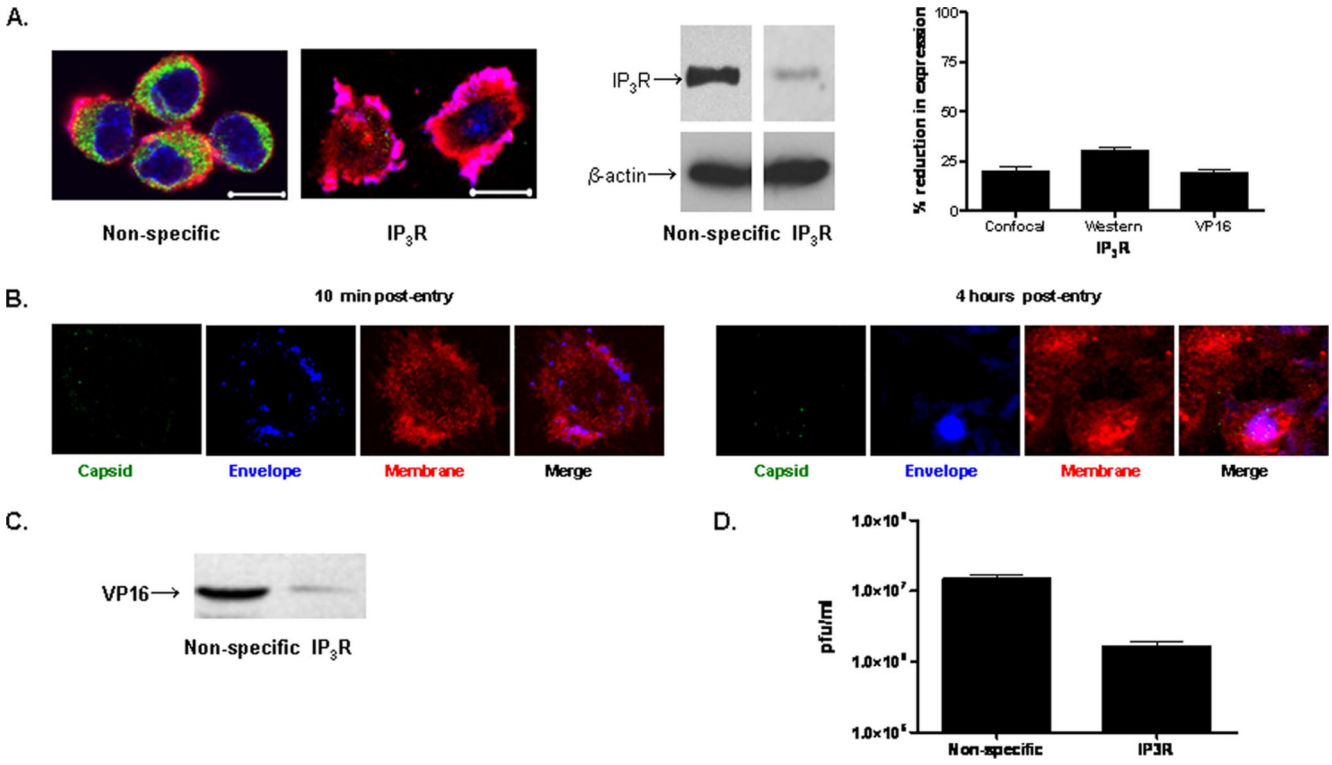

Figure 6. Blockade of IP_3R with siRNA Prevents HSV Entry. (A) Cells were transfected with nonspecific or a combination of IP_3R-specific siRNAs targeting all three isoforms, and 48 h after transfection, cells were stained with a mAb to the IP_3Rs (green) and examined by confocal microscopy (membranes, red; and nucleus, blue) (left). Alternatively, Western blots of cell lysates were prepared 48 h after transfection. Representative blots from three independent experiments are shown (middle). Blots and confocal images were quantified as described in Figure 2. (B) Transfected CaSki cells were infected with DiD-labeled K26GFP virus (moi = 5), and 10 min and 4 h after infection, the cells were fixed, stained, and viewed by confocal microscopy (red, plasma membrane, blue, viral envelope; green, viral capsid; VP26, purple, colocalization of plasma membrane and viral envelope). Results are representative of those obtained with ~100 cells in three independent experiments. (C) Transfected CaSki cells were exposed to HSV-2(G) (moi = 1) in a synchronized infection assay, and 1 h postcitrate treatment, nuclear extracts were prepared and analyzed for VP16 by Western blotting. Results shown are representative of three independent experiments. Blots were scanned, and nuclear VP16 detected in siRNA-transfected cells as a percentage of VP16 detected in nonspecific siRNA-transfected cells was compared (A, right). (D) Transfected cells were exposed to serial dilutions of HSV-2(G) 48 h after transfection. Plaques were counted 48 h pi, and viral titer was determined. Results are means ± SD of three independent experiments conducted in duplicate.

the gD$^-$ virus, the viral envelope (blue) colocalizes with both the cell membrane (red) and integrinαv (green). In contrast, after infection with gH$^-$ virus, no colocalization with integrin is observed. These findings suggest that gH interacts with integrinαv, even in the absence of gD. Notably, integrinαv seems to clump together with the viral envelope at the cell membrane after exposure to the gD$^-$, but not the gH$^-$, virus. We previously used calcium fluorometry and pharmacological agents to examine the Ca^{2+} response to HSV. Although fluorometry provides quantitative data on the intracellular Ca^{2+} concentration, the cellular source cannot be easily determined. Additionally, pharmacological agents are relatively nonspecific and have multiple effects. To overcome these limitations, we used confocal microscopy coupled with siRNA targeting of the IP_3Rs to further define the role Ca^{2+} plays in viral infection. Activation of IP_3Rs triggers Ca^{2+} release mostly from the ER, although some cells express IP_3R isoforms in their plasma membrane (Tanimura *et al*., 2000). Three different isoforms of the IP_3R may be expressed. Transfection of CaSki cells with a combination of IP_3R sequence-specific siRNAs directed at all three isoforms reduced IP_3R expression by 70–80% (based on scanning of confocal microscopy images and Western blots) (Figure 6A). The impact on viral entry was monitored by confocal microscopy with dually labeled virus. No internalized GFP was detected in cells transfected with IP_3R-specific siRNA at any time pi (compare Figure 6B with 4B, top). Rather, the viral envelope seemed to fuse with the cell membrane, but it remained trapped at the membrane. Consistent with the confocal images, nuclear transport of VP 16 was reduced by 81% (Figure 6C) and viral yields by 89% (Figure 6D). We previously reported that HSV preferentially infects the apical surface of polarized ECC-1 cells and that nectin-1 sorted to the apical surface of these cells (Galen *et al*., 2006). We expanded this work by also examining the polarity of expression of syndecan-2, integrinαv, and IP_3R on ECC-1 cells. Confocal images demonstrated that syndecan-2 preferentially sorted to the basal surface of cells, although the core proteoglycan was readily detected at both membranes. In contrast, nectin-1, integrinαv, and IP_3R preferentially sorted to the apical membrane of cells (Figure 7A). Moreover, when cells that had been grown on Transwells and loaded with Calcium Green were exposed to HSV-2(G) from the apical or basolateral membrane, Ca^{2+} release was observed almost exclusively after apical exposure (Figure 7B). These observations are consistent with previous studies with polarized pancreatic acinar cells and enterocytes (Nathanson *et al*., 1994; Matovcik *et al*., 1996; Yamamoto-Hino *et al*., 1998), which demonstrate that IP_3R are concentrated near the apical pole of the cell membrane and indicate that the preferential apical expression of nectin-1, integrinαv, and IP_3R may contribute to the observation that HSV preferentially infects the apical surface of ECC-1 cells (Galen *et al*., 2006). Syndecans interact with cytoskeletal proteins including integrins to facilitate cell attachment and motility (Bishop *et al*., 2007). To explore the relationship between these cellular proteins, the subcellular localization of integrinαv after syndecan-2 siRNA

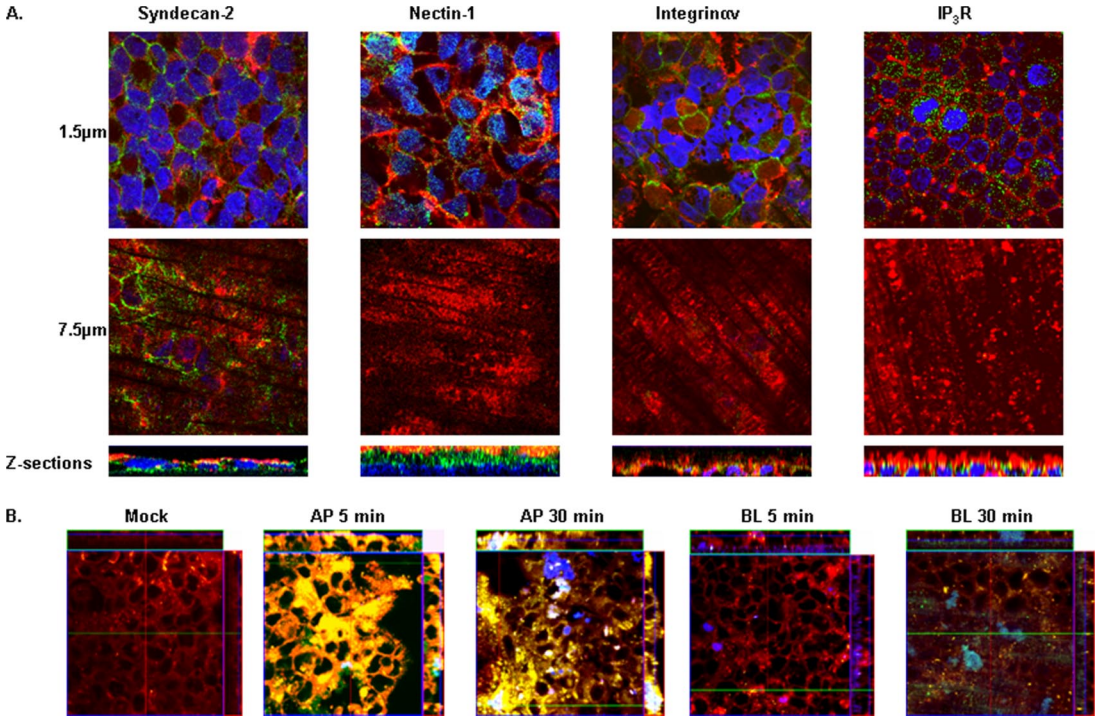

Figure 7. Polarized expression of receptors on ECC-1 cells. (A) ECC-1 cells were grown on Transwells and stained with EZ-Link Sulfo-NHS-Biotin to detect cellular plasma membranes (red). Then, they were permeabilized, and the nuclei were detected by DAPI (blue). Syndecan, nectin-1, integrinαv, and IP_3R were visualized by labeling each with a cocktail of specific mAbs (green). Successive axial sections from the apical to the basal membrane were obtained; the axial images 1.5 and 7.5 μm from the apical surface and Z-sections are representative of at least five independent experiments. (B) Representative XYZ-section images of Calcium Green–loaded polarized ECC-1 cells after infection from either the apical (AP) or basolateral membrane (BL) with DiD-labeled HSV-2(G). Cells were fixed and stained 5 or 30 min after infection (plasma membrane, red; viral envelope, blue; calcium, green; colocalization of calcium and plasma membranes, yellow; colocalization of membrane and envelope, purple; and colocalization of envelope and calcium, turquoise). Results are representative of those obtained in three independent experiments.

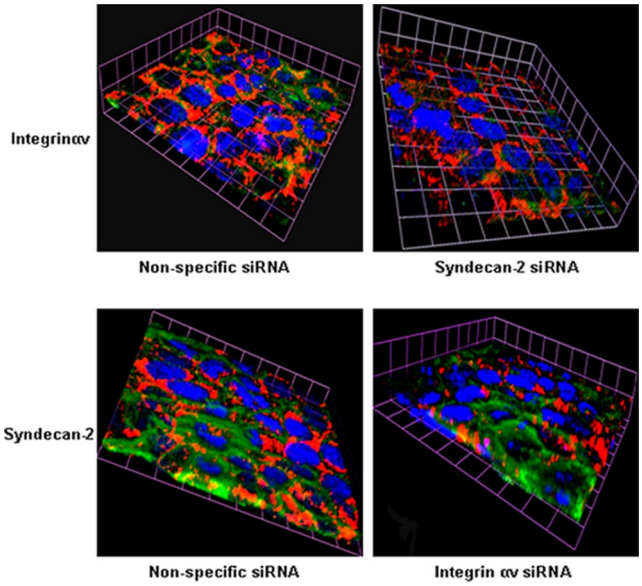

Figure 8. Gene silencing of syndecan-2 alters subcellular localization of integrinαv. CaSki cells were transfected with nonspecific and syndecan-2–specific siRNA and 48 h later, fixed, and stained for expression of integrinαv (green), plasma membrane (red) and nuclei (blue) (top). Conversely, cells were transfected with nonspecific or integrinαv-specific siRNA, and then they were fixed and stained for expression of syndecan-2 (green) (bottom). The 3-D images are representative of results obtained from two independent experiments.

knockdown, and conversely, the localization of syndecan-2 after siRNA integrinαv knockdown were evaluated. Gene silencing of syndecan-2 resulted in a change in integrinαv subcellular localization with less integrin being detected at the plasma membrane. In contrast, silencing of integrinαv had little impact on syndecan-2 expression (Figure 8). Knockdown of syndecan-2 also modified localization of nectin-1, whereas knockdown of nectin had little impact on syndecan-2 (data not shown). The dependence of integrin (and nectin) localization on syndecan protein expression is consistent with the known interactions between these proteins in other biological systems. For example, fibronectin binds simultaneously to heparan sulfate chains of syndecan and one or more integrins to induce cell spreading and focal adhesion formation (Couchman *et al*., 2001). Similarly, HSV may interact with heparan sulfate chains of syndecan, nectin, and integrins to form a functional complex that facilitates viral entry.

Syndecan-2, Nectin-1, Integrinαv, and IP_3R Differentially Contribute to HSV-induced Ca^{2+} Signaling

Having established a role for these cellular proteins in viral entry, the impact of each on the Ca^{2+} responses was evaluated. No increase in membrane-associated or global Ca^{2+} was observed in cells transfected with syndecan-2 siRNA, consistent with the marked reduction in viral binding (Figure 9A, top). Bound virus (blue) was observed in cells transfected with nectin siRNA, but, consistent with the results obtained with the gD^- virus (Figure 1B), in the absence of nectin, no membrane or global Ca^{2+} response was elicited. However, increases in membrane, but not global, Ca^{2+} were observed in cells transfected with siRNA targeting integrinαv or IP_3R. The source of the changes in membrane Ca^{2+} could represent release from stores within or just beneath the membrane, but it is unlikely to reflect influx of extracellular Ca^{2+}, because the cells were washed three times with Ca^{2+}-free PBS before shifting the temperature to 37°C. These findings are consistent with results obtained with the gH^- virus, and they suggest that engagement of syndecan and nectin alone is sufficient to trigger membrane Ca^{2+} responses, but the global Ca^{2+} response requires signaling through integrinαv and activation of IP_3R. Infection of cells transfected with nonspecific siRNA or an unrelated siRNA targeting HVEM (bottom) elicited both the membrane and global intracellular Ca^{2+} response. We also examined the viral-induced Ca^{2+} signaling response by excitation ratio fluorometry of cells loaded with Ca^{2+} indicator, fura-2. Exposure of cells transfected with nonspecific siRNA resulted in a significant rapid increase in $[Ca^{2+}]_i$, which peaked within 1 min (Figure 9, B and C; $p < 0.001$). A blunted, albeit significant increase in $[Ca^{2+}]_i$, was also observed after transfection with either integrinαv or IP_3R siRNA, reflecting the membrane Ca^{2+} response. No significant increases in $[Ca^{2+}]_i$ were observed in cells transfected with either of the other siRNAs or in CHOK1 cells.

DISCUSSION

These studies demonstrate that HSV triggers release of two distinct intracellular Ca^{2+} stores, membrane and global IP_3R-sensitive intracellular Ca^{2+}, which are required for viral entry into human epithelial cells. The mobilization of membrane Ca^{2+} is triggered by interactions between the viral envelope and heparan sulfate glycosaminoglycan chains of syndecan-2 and nectin-1 coreceptors, but alone, it is not sufficient for viral entry. Engagement of integrinαv and activation of IP_3Rs are required to trigger the release of global Ca^{2+} stores and to promote completion of the penetration process and the intracellular delivery of viral capsids. The identification of heparan sulfate proteoglycans as receptors for HSV attachment is well documented (WuDunn and Spear, 1989; Shieh *et al*., 1992). However, no studies have addressed which family of proteoglycans is involved. Recent work demonstrated that human cervical and vaginal epithelia express high levels of syndecan-1 and -2, with little expression of syndecan-3 and-4 or glypicans (Bobardt *et al*., 2007). Consistent with this notion, we found that transfection of human cervical epithelial cells with siRNA specific for syndecan-2 had the greatest impact on HSV binding and infection and abrogated the membrane and global Ca^{2+} responses. Transfection with syndecan-1 siRNA had more modest effects on viral binding and infection. No glypican was detected. Notably, human immunodeficiency virus (HIV) also interacts with syndecans to bind to primary human genital tract epithelial cells (Bobardt *et al*., 2007). Thus, targeting syndecans, either through siRNA or other strategies, could provide a novel mechanism to reduce transmission of HSV and HIV. Although ligation of syndecan receptors by some proteins triggers a signaling response (Bernfield *et al*., 1999), binding of HSV to syndecan is not sufficient to trigger any Ca^{2+} response or to mediate viral entry. Activation of membrane Ca^{2+} by HSV also requires engagement of nectin coreceptors. Cells express a variety of Ca^{2+} channels in their membrane, which contribute to the subplasma membrane Ca^{2+} microdomains (Rizzuto and Pozzan, 2006). Although these membrane Ca^{2+} transients are primarily due to opening of these channels, they also may be generated from IP_3R-sensitive intracellular Ca^{2+} stores near the membrane (Tanimura *et al*., 2000) or to apical secretory granules, as described in pancreatic acinar cells (Gerasimenko *et al*.,

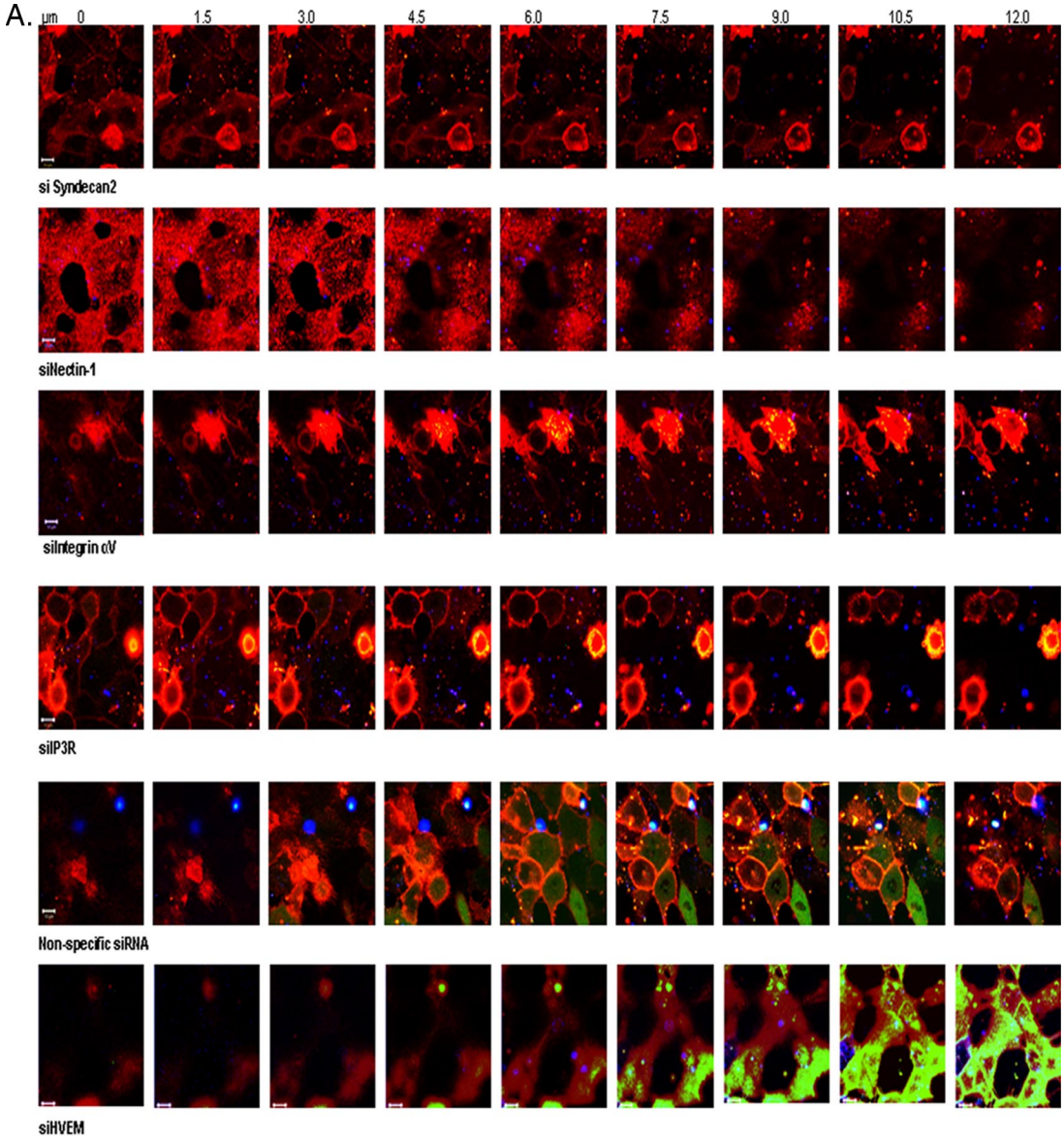
A.
μm 0
1.5
3.0
4.5
6.0
7.5
9.0
10.5
12.0
si Syndecan2
siNectin-1
siIntegrin αV
siIP3R
Non-specific siRNA
siHVEM
B.
nonsiRNA
IP3R siRNA
HSV-2(G)
[Ca2+] nM
time (sec)
C.
[Ca2+]i nM
Basal
Peak
Non-Specific
siSyndecan
siNectin
siIntegrin
siIP3R
CHOK1

2006). However, siRNA blockade of IP_3R failed to abolish the membrane Ca^{2+} response to HSV, suggesting that IP_3R-sensitive stores are not the source of the observed HSV-triggered membrane Ca^{2+} response. Further studies to define the nature of this membrane response are in progress. The observation that the HSV-mediated release of global Ca^{2+} involves integrin receptors is consistent with prior observations that integrin ligands modulate Ca^{2+} homeostasis (Somogyi *et al*., 1994; Chan *et al*., 2001). A role for integrins in HSV invasion is also consistent with prior observations demonstrating that HSV activates the phosphorylation of FAK and other tyrosine kinases to promote viral capsid transport toward the nucleus (Qie *et al*., 1999; Cheshenko *et al*., 2005). Cross talk between integrins and FAK, which directly binds to the cytoplasmic tail of integrins, is well documented (Mitra and Schlaepfer, 2006). The confocal studies with deletion viruses support the notion that gH is a ligand for integrinαv (Figure 5). In a previous study, a pronounced inhibitory effect was observed with anti-integrinαv antibodies, suggesting a role for αv integrin subunits in HSV entry (Parry *et al*., 2005). CHO cells expressing human $\alpha v\beta 3$ integrin molecules bound efficiently to wild-type recombinant gH–gL, but they did not bind to a modified gH–gL in which the integrin-binding motif had been mutated to Arg-Gly-Glu (RGE) (Parry *et al*., 2005). These studies suggest that the RGD sequence mediates binding to $\alpha v\beta 3$ integrin molecules. However, a recombinant virus in which the RGD motif was mutated to RGE was not impaired for infection (Galdiero *et al*., 1997), and RGD peptides failed to block infection (Israel *et al*., 1998). Possibly, there are other domains within gH that mediate binding to integrinαv molecules and may recognize other β-subunits. Studies are underway to determine whether there are specific β-subunit(s) that participate in this HSV induced signaling. The notion that engagement of syndecans, nectin and integrins converge to activate a signaling pathway is consistent with known interactions between these different proteins. Interactions between syndecans and integrins and nectin and integrins to form signaling complexes is well described (Couchman *et al*., 2001; Woods and Couchman, 2001; Thodeti *et al*., 2003; Beauvais *et al*., 2004; Beauvais and Rapraeger, 2004). Specifically, the ectodomain of syndecan-1 core protein contains an active site that assembles into a complex with $\alpha v\beta 5$ integrins to regulate integrin activity. Similarly, nectin-1 and nectin-3 molecules colocalize with $\alpha v\beta 5$ integrins at adherens junctions (Ikeda *et al*., 2004; Kakunaga *et al*., 2004; Sakamoto *et al*., 2006). Integrins transduce signals inside the cells, which induce the reorganization of the actin cytoskeleton, eventually causing integrin clustering and formation of cell–matrix junctions such as focal complexes and focal adhesions. It is notable, therefore, that interactions of gH-expressing HSV with integrin (Figure 5) led to clustering of integrin receptors, which may induce changes in the cytoskeleton that promote completion of the viral entry process. Interactions between these cellular receptors is also supported by the observation that silencing of syndecan-2 modified the subcellular localization of nectin and integrinαv (Fig. 8). In the polarized epithelial cells studied, Ca^{2+} waves typically originate from the apical pole, where IP_3Rs are clustered (Matovcik *et al*., 1996; Nakanishi *et al*., 1996), (Lee *et al*., 1997; Yule *et al*., 1997; Zhang *et al*., 1997). Consistent with this notion, we found that both integrinαv and IP_3Rs cluster at the apical membrane in human uterine epithelial cells grown under polarizing conditions and release Ca^{2+} apically. These findings provide another potential mechanism to explain our recent work demonstrating that HSV preferentially infects the apical surface of ECC-1 and other human epithelial cell types (Galen *et al*., 2006). In those studies, we found that nectin-1 polarizes to the apical surface, contributing to preferential apical entry of HSV. Although syndecan-2 is sorted preferentially to the basolateral membrane of these polarized cells, sufficient protein is found apically to support viral binding. Together, these studies suggest that the cellular components involved in HSV entry may cluster at the apical pole to form signaling complexes. In summary these studies identify for the first time that HSV triggers two discrete Ca^{2+} signaling responses. Binding to syndecan and engagement of nectin by gD trigger release of plasma membrane Ca^{2+} stores, which may be involved in the initiation of viral fusion. However, completion of the penetration process and the intracellular release of viral capsids require engagement of integrinαv subunits by gH and release of IP_3R sensitive intracellular Ca^{2+} stores. Blocking this Ca^{2+} signaling pathway at any step significantly inhibits HSV entry and infection, thus identifying novel targets for prevention strategies.

Figure 9 (facing page). HSV triggers membrane Ca^{2+} release if syndecan and nectin are present, but requires integrinαv and IP_3R for the global Ca^{2+} response. (A) CaSki cell membranes were labeled with VYBRANT-DiI (red) and transfected with nonspecific or specific siRNAs as indicated. Forty-eight hours after transfection, the cells were loaded with Calcium Green and infected in a synchronized assay with DiD-envelope–labeled HSV-2(G) (blue). Live images were acquired at 1-s intervals pi at the indicated slice size. Representative images obtained 2 s after the temperature reached 37°C are shown. (B) CaSki cells were transfected with nonspecific or IP_3R siRNAs and 48 h later, cells were loaded with the Ca^{2+} indicator dye Fura-2, exposed to HSV-2(G) (moi = 10) and changes in $[Ca^{2+}]_i$ monitored. Representative results from a single experiment showing two individual cells are displayed. (C) The bar graph depicts changes in $[Ca^{2+}]_i$ elicited by HSV-2(G) on CaSki cells transfected with the indicated siRNA or CHOK1 cells. Means obtained from at least two independent experiments monitoring at least 10 cells are depicted, and the error bars indicate SE; asterisks indicate significant differences between baseline and peak Ca^{2+} response to HSV by paired *t* tests ($p < 0.001$).

ACKNOWLEDGMENTS

We thank Prashant Desai (Johns Hopkins University) for the K26GFP virus. Confocal laser scanning microscopy was performed at the Mount Sinai School of Medicine Microscopy Shared Resource Facility, supported with funding from National Institutes of Health (NIH)-National Cancer Institute shared resources grant 5R24 CA095823-04), National Science Foundation Major Research Instrumentation grant DBI-9724504, and NIH shared instrumentation grant 1 S10 RPO 9145-01. We thank Rumana Hug and Paul Chao for technical assistance and advice. This work was supported by NIH grants AI061679 (to B.C.H.), AI70202 (to B.C.H.), DK38470 (to L.M.S.), and DK62345 (to L.M.S.). W.L. was supported by a Fellowship Grant from the Polycystic Kidney Research Foundation.

REFERENCES

Beauvais, D. M., Burbach, B. J., and Rapraeger, A. C. (2004). The syndecan-1 ectodomain regulates alphavbeta3 integrin activity in human mammary carcinoma cells. J. Cell Biol. *167*, 171–181.

Beauvais, D. M., and Rapraeger, A. C. (2004). Syndecans in tumor cell adhesion and signaling. Reprod. Biol. Endocrinol. *2*, 3.

Bernfield, M., Gotte, M., Park, P. W., Reizes, O., Fitzgerald, M. L., Lincecum, J., and Zako, M. (1999). Functions of cell surface heparan sulfate proteoglycans. Annu. Rev. Biochem. *68*, 729–777.

Berridge, M. J. (2005). Unlocking the secrets of cell signaling. Annu. Rev. Physiol. *67*, 1–21.

Bishop, J. R., Schuksz, M., and Esko, J. D. (2007). Heparan sulphate proteoglycans fine-tune mammalian physiology. Nature *446*, 1030–1037.

Bobardt, M., Chatterji, U, Selvarajah, S, Van der Schueren, B., David, G, Kahn, B an Gallay, P. A. (2007). Cell-free HIV-1 transcytosis through primary genital epithelial cells. J. Virol. *81*, 395–405.

Chan, W. L., Holstein-Rathlou, N. H., and Yip, K. P. (2001). Integrin mobilizes intracellular Ca(2+) in renal vascular smooth muscle cells. Am. J. Physiol. *280*, C593–C603.

Cheshenko, N., Del Rosario, B., Woda, C., Marcellino, D., Satlin, L. M., and Herold, B. C. (2003). Herpes simplex virus triggers activation of calcium-signaling pathways. J. Cell Biol. *163*, 283–293.

Cheshenko, N., and Herold, B. C. (2002). Glycoprotein B plays a predominant role in mediating herpes simplex virus type 2 attachment and is required for entry and cell-to-cell spread. J. Gen. Virol. *83*, 2247–2255.

Cheshenko, N., Liu, W., Satlin, L. M., and Herold, B. C. (2005). Focal adhesion kinase plays a pivotal role in herpes simplex virus entry. J. Biol. Chem. *280*, 31116–31125.

Couchman, J. R., Chen, L., and Woods, A. (2001). Syndecans and cell adhesion. Int. Rev. Cytol. *207*, 113–150.

Desai, P., and Person, S. (1998). Incorporation of the green fluorescent protein into the herpes simplex virus type 1 capsid. J. Virol. *72*, 7563–7568.

Forrester, A., Farrell, H., Wilkinson, G., Kaye, J., Davis-Poynter, N., and Minson, T. (1992). Construction and properties of a mutant of herpes simplex virus type 1 with glycoprotein H coding sequences deleted. J. Virol. *66*, 341–348.

Galdiero, M., Whiteley, A., Bruun, B., Bell, S., Minson, T., and Browne, H. (1997). Site-directed and linker insertion mutagenesis of herpes simplex virus type 1 glycoprotein H. J. Virol. *71*, 2163–2170.

Galen, B., Cheshenko, N., Tuyama, A., Ramratnam, B., and Herold, B. C. (2006). Access to nectin favors herpes simplex virus infection at the apical surface of polarized human epithelial cells. J. Virol. *80*, 12209–12218.

Gerasimenko, J. V., Flowerdew, S. E., Voronina, S. G., Sukhomlin, T. K., Tepikin, A. V., Petersen, O. H., and Gerasimenko, O. V. (2006). Bile acids induce Ca^{2+} release from both the endoplasmic reticulum and acidic intracellular calcium stores through activation of inositol trisphosphate receptors and ryanodine receptors. J. Biol. Chem. *281*, 40154–40163.

Gerber, S. I., Belval, B. J., and Herold, B. C. (1995). Differences in the role of glycoprotein C of HSV-1 and HSV-2 in viral binding may contribute to serotype differences in cell tropism. Virology *214*, 29–39.

Giancotti, F. G., and Ruoslahti, E. (1999). Integrin signaling. Science *285*, 1028–1032.

Gianni, T., Menotti, L., and Campadelli-Fiume, G. (2005). A heptad repeat in herpes simplex virus 1 gH, located downstream of the alpha-helix with attributes of a fusion peptide, is critical for virus entry and fusion. J. Virol. *79*, 7042–7049.

Gianni, T., Piccoli, A., Bertucci, C., and Campadelli-Fiume, G. (2006). Heptad repeat 2 in herpes simplex virus 1 gH interacts with heptad repeat 1 and is critical for virus entry and fusion. J. Virol. *80*, 2216–2224.

Herold, B. C., WuDunn, D., Soltys, N., and Spear, P. G. (1991). Glycoprotein C of herpes simplex virus type 1 plays a principal role in the adsorption of virus to cells and in infectivity. J. Virol. *65*, 1090–1098.

Ikeda, W., Kakunaga, S., Takekuni, K., Shingai, T., Satoh, K., Morimoto, K., Takeuchi, M., Imai, T., and Takai, Y. (2004). Nectin-like molecule-5/Tage4 enhances cell migration in an integrin-dependent, Nectin-3-independent manner. J. Biol. Chem. *279*, 18015–18025.

Israel, B. A., Schultz, K. T., and Murphy, C. J. (1998). Lack of detectable interaction between HSV-1 and integrins or tachykinins. Intervirology *41*, 132–134.

Kakunaga, S., Ikeda, W., Shingai, T., Fujito, T., Yamada, A., Minami, Y., Imai, T., and Takai, Y. (2004). Enhancement of serum- and platelet-derived growth factor-induced cell proliferation by Necl-5/Tage4/poliovirus receptor/CD155 through the Ras-Raf-MEK-ERK signaling. J. Biol. Chem. *279*, 36419–36425.

Lakadamyali, M., Rust, M. J., Babcock, H. P., and Zhuang, X. (2003). Visualizing infection of individual influenza viruses. Proc. Natl. Acad. Sci. USA *100*, 9280–9285.

Le Blanc, I. *et al*. (2005). Endosome-to-cytosol transport of viral nucleocapsids. Nat. Cell Biol. *7*, 653–664.

Lee, M. G., Xu, X., Zeng, W., Diaz, J., Kuo, T. H., Wuytack, F., Racymaekers, L., and Muallem, S. (1997). Polarized expression of Ca2+ pumps in pancreatic and salivary gland cells. Role in initiation and propagation of [Ca2+]i waves. J. Biol. Chem. *272*, 15771–15776.

Ligas, M. W., and Johnson, D. C. (1988). A herpes simplex virus mutant in which glycoprotein D sequences are replaced by beta-galactosidase sequences binds to but is unable to penetrate into cells. J. Virol. *62*, 1486–1494.

Linehan, M. M., Richman, S., Krummenacher, C., Eisenberg, R. J., Cohen, G. H., and Iwasaki, A. (2004). In vivo role of nectin-1 in entry of herpes simplex virus type 1 (HSV-1) and HSV-2 through the vaginal mucosa. J. Virol. *78*, 2530–2536.

Matovcik, L. M., Maranto, A. R., Soroka, C. J., Gorelick, F. S., Smith, J., and Goldenring, J. R. (1996). Co-distribution of calmodulin-dependent protein kinase II and inositol trisphosphate receptors in an apical domain of gastrointestinal mucosal cells. J. Histochem. Cytochem. *44*, 1243–1250.

Mitra, S. K., and Schlaepfer, D. D. (2006). Integrin-regulated FAK-Src signaling in normal and cancer cells. Curr. Opin. Cell Biol. *18*, 516–523.

Montgomery, R. I., Warner, M. S., Lum, B. J., and Spear, P. G. (1996). Herpes simplex virus-1 entry into cells mediated by a novel member of the TNF/NGF receptor family. Cell *87*, 427–436.

Nakanishi, S., Fujii, A., Nakade, S., and Mikoshiba, K. (1996). Immunohistochemical localization of inositol 1,4,5-trisphosphate receptors in non-neural tissues, with special reference to epithelia, the reproductive system, and muscular tissues. Cell Tissue Res. *285*, 235–251.

Nathanson, M. H., Burgstahler, A. D., and Fallon, M. B. (1994). Multistep mechanism of polarized Ca2+ wave patterns in hepatocytes. Am. J. Physiol. *267*, G338–349.

Parry, C., Bell, S., Minson, T., and Browne, H. (2005). Herpes simplex virus type 1 glycoprotein H binds to alphavbeta3 integrins. J. Gen. Virol. *86*, 7–10.

Qie, L., Marcellino, D., and Herold, B. C. (1999). Herpes simplex virus entry is associated with tyrosine phosphorylation of cellular proteins. Virology *256*, 220–227.

Rizzuto, R., and Pozzan, T. (2006). Microdomains of intracellular Ca2+: molecular determinants and functional consequences. Physiol. Rev. *86*, 369–408.

Sakamoto, Y., Ogita, H., Hirota, T., Kawakatsu, T., Fukuyama, T., Yasumi, M., Kanzaki, N., Ozaki, M., and Takai, Y. (2006). Interaction of integrin alpha(v-)beta3 with nectin. Implication in cross-talk between cell-matrix and cell-cell junctions. J. Biol. Chem. *281*, 19631–19644.

Schaefer, T. M., Desouza, K., Fahey, J. V., Beagley, K. W., and Wira, C. R. (2004). Toll-like receptor (TLR) expression and TLR-mediated cytokine/chemokine production by human uterine epithelial cells. Immunology *112*, 428–436.

Shieh, M. T., WuDunn, D., Montgomery, R. I., Esko, J. D., and Spear, P. G. (1992). Cell surface receptors for herpes simplex virus are heparan sulfate proteoglycans. J. Cell Biol. *116*, 1273–1281.

Somogyi, L., Lasic, Z., Vukicevic, S., and Banfic, H. (1994). Collagen type IV stimulates an increase in intracellular Ca2+ in pancreatic acinar cells via activation of phospholipase C. Biochem. J. *299*, 603–611.

Spear, P. G. (2004). Herpes simplex virus: receptors and ligands for cell entry. Cell Microbiol. *6*, 401–410.

Tanimura, A., Tojyo, Y., and Turner, R. J. (2000). Evidence that type I, II, and III inositol 1,4,5-trisphosphate receptors can occur as integral plasma membrane proteins. J. Biol. Chem. *275*, 27488–27493.

Thodeti, C. K., Albrechtsen, R., Grauslund, M., Asmar, M., Larsson, C., Takada, Y., Mercurio, A. M., Couchman, J. R., and Wewer, U. M. (2003). ADAM12/syndecan-4 signaling promotes beta 1 integrin-dependent cell spreading through protein kinase Calpha and RhoA. J. Biol. Chem. *278*, 9576–9584.

Tuyama, A. C. *et al*. (2006). ACIDFORM inactivates herpes simplex virus and prevents genital herpes in a mouse model: optimal candidate for microbicide combinations. J. Infect. Dis. *194*, 795–803.

Warner, M. S., Geraghty, R. J., Martinez, W. M., Montgomery, R. I., Whitbeck, J. C., Xu, R., Eisenberg, R. J., Cohen, G. H., and Spear, P. G. (1998). A cell surface protein with herpesvirus entry activity (HveB) confers susceptibility to infection by mutants of herpes simplex virus type 1, herpes simplex virus type 2, and pseudorabies virus. Virology *246*, 179–189.

Woods, A., and Couchman, J. R. (2001). Syndecan-4 and focal adhesion function. Curr. Opin. Cell Biol. *13*, 578–583.

WuDunn, D., and Spear, P. G. (1989). Initial interaction of herpes simplex virus with cells is binding to heparan sulfate. J. Virol. *63*, 52–58.

Yamamoto-Hino, M., Miyawaki, A., Segawa, A., Adachi, E., Yamashina, S., Fujimoto, T., Sugiyama, T., Furuichi, T., Hasegawa, M., and Mikoshiba, K. (1998). Apical vesicles bearing inositol 1,4,5-trisphosphate receptors in the Ca2+ initiation site of ductal epithelium of submandibular gland. J. Cell Biol. *141*, 135–142.

Yule, D. I., Ernst, S. A., Ohnishi, H., and Wojcikiewicz, R. J. (1997). Evidence that zymogen granules are not a physiologically relevant calcium pool. Defining the distribution of inositol 1,4,5-trisphosphate receptors in pancreatic acinar cells. J. Biol. Chem. *272*, 9093–9098.

Zhang, X., Wen, J., Bidasee, K. R., Besch, H. R., Jr., and Rubin, R. P. (1997). Ryanodine receptor expression is associated with intracellular Ca2+ release in rat parotid acinar cells. Am. J. Physiol. *273*, C1306–C1314.